SCIENTIFIC Publishing Limited

New Energy Exploitation and Application

https://ojs.ukscip.com/index.php/neea

Article

Climate Aware Reliability Analysis of Renewable Energy Systems Using Nonstationary Stochastic Hazard Models

Janardan Behera

Department of Statistics, Ravenshaw University, Kataka 753003, India; janardanbeheragreetsyou@gmail.com or janardan@ravenshawuniversity.ac.in

Received: 2 August 2026; **Revised:** 10 October 2026; **Accepted:** 19 October 2026; **Published:** 3 November 2026

Abstract: Renewable energy assets are certified against hazard functions that classical reliability theory treats as fixed in time, yet the climate driving heat stress, humidity, wind extremes, and flooding is shifting in ways that make stationarity untenable for long-lived infrastructure. This article develops a hazard model in which asset failure intensity combines a Weibull baseline for intrinsic wear with a climate-driven component following an affine jump diffusion, joining mean-reverting drift from gradual thermal and humidity loading with discrete jumps from cyclones and floods. A closed-form reliability function is derived through a Riccati equation, transferring machinery from interest rate, credit risk, and stochastic mortality modeling to infrastructure reliability, and is extended to trending climate means and extreme event frequencies through a time-inhomogeneous quadrature formula. The model yields a Climate Resilience Index and agrees with forty thousand path Monte Carlo simulations within one third of one percent over sixty years. Calibrated applications to solar photovoltaic arrays, wind turbines, battery storage units, and coastal transmission towers, grounded in published Indian degradation and cyclone fragility data, show that climate-driven hazard erodes mean time to failure most severely for cyclone-exposed transmission towers, whose lifetime resilience index in coastal Odisha falls from 0.44 under a stationary climate to 0.36 under severe warming, and least severely for enclosed battery systems.

Keywords: Climate Aware Reliability; Renewable Energy Systems; Affine Jump Diffusion; Nonstationary Hazard Models; Weibull Reliability; Climate Resilience Index; Extreme Weather Risk; Monte Carlo Simulation

1. Introduction

1.1. Background

The global renewable energy fleet has grown from a marginal contribution to electricity supply into a structural pillar of national power systems within little more than a decade, and the pace of that expansion is not expected to slow. Solar photovoltaic capacity, wind generation, and grid-scale battery storage are now routinely sited in environments that were never part of the design basis against which their components were originally certified. At the same time, the climate system that these assets must operate within is no longer the stationary backdrop that engineering standards implicitly assume. The Sixth Assessment Report of the Intergovernmental Panel on Climate Change concludes that human-caused climate change is already affecting many weather and climate extremes in every region of the globe [1], and recent reviews document that weather-driven stress on power grid components is rising [2]. Sea surface temperatures have risen enough to measurably intensify tropical cyclone wind fields, the fifty-year return period wind speed used to classify offshore and coastal wind turbines has increased across most of the world's oceans over the past several decades, and humid heat extremes that accelerate polymer and semicon-

ductor degradation in solar modules are becoming more frequent in exactly the geographies where solar capacity is expanding fastest, a pattern documented in detail in Section 2.2 below. Renewable energy reliability has historically been assessed using hazard functions calibrated to historical failure data under the implicit assumption that the environment generating those failures will continue to behave as it did during the calibration period. That assumption is increasingly difficult to defend.

The consequences of treating climate as stationary are not abstract. When Cyclone Fani made landfall on the Odisha coast in 2019, eighty-seven high-voltage transmission towers collapsed outright and a further forty-one suffered partial damage, according to the record that the Odisha Power Transmission Corporation Limited released to Raj et al. [3], a record examined closely in the case study of Section 7. The loss to the transmission and distribution system was reported at roughly eight thousand crore rupees [3], and many consumers experienced prolonged outages. Photovoltaic modules operating in composite Indian climates have been measured losing electrical output at rates that vary by more than an order of magnitude across competing cell technologies depending on how each technology tolerates sustained heat and humidity, evidence reviewed in Section 2.2. These are not isolated engineering anecdotes. They are observations of a hazard process that is dynamic, asset-specific, and tied to a climate system whose statistical properties are themselves moving.

1.2. Motivation

Reliability engineering possesses a mature and powerful toolkit for handling time-varying failure rates, built around the Weibull family, a proportional hazards regression tradition reviewed in Section 2.1, and a long tradition of survival analysis recast explicitly as a theory of stochastic processes. What this toolkit was not built to handle, at least not in its classical form, is a covariate process whose own statistical law is changing over the asset lifetime in a way that compounds with the random arrival of discrete extreme events. A wind turbine commissioned today faces a fifty-year return period wind speed at the end of its life that is, in many coastal basins, measurably higher than the one used in its design certification, and the difference is not a fixed offset but a trend that is itself uncertain. A transmission corridor built to withstand the cyclone climatology of the 1980s is being asked to survive a Bay of Bengal cyclone climatology that has already produced storms outside that historical envelope [4]. Treating the climate covariate as fixed, or even as a stationary stochastic process with constant statistical moments, discards exactly the information that motivates building a climate-aware model in the first place. Work on infrastructure risk in a changing climate has begun to replace homogeneous Poisson hazard models with nonstationary point processes [5], but those models stop at the hazard arrival stage and do not produce a reliability function that also carries gradual wear and continuous climate loading.

The mathematical machinery required to handle a hazard rate that is itself a stochastic process with both continuous and jump components already exists, though it was developed for a different purpose, a lineage traced in full in Section 2.3. Interest rate modeling solved an analogous problem decades ago when the short rate driving bond prices was recognized to be better described as a mean-reverting diffusion than as a deterministic curve, and a square root diffusion produced the first widely used closed-form solution for the resulting discount factor. Credit risk theory subsequently recognized that default arrival could be modeled the same way, treating the default intensity as a doubly stochastic Cox process whose survival probability inherits the same affine tractability. Actuarial science completed the analogy by applying the identical machinery to human mortality, replacing a fixed life table with a stochastic mortality intensity that admits closed-form survival probabilities through transform methods developed for the broader affine jump diffusion class [6]. No comparable transfer has yet been made into engineering reliability for renewable energy infrastructure, despite the underlying mathematical structure being essentially identical to the one needed here, namely a positive intensity process whose integral determines a survival probability.

1.3. Research Gap

Three assumptions recur across the climate and energy literature reviewed in Section 2 and across the reliability literature on which renewable asset certification still largely rests. Failure intensities are treated as constant or as deterministic functions of age alone. Environmental conditions entering the hazard function, where they enter at all, are treated as stationary. Discrete extreme events such as cyclone landfalls are either ignored or folded into an average annual exceedance probability that erases the clustering and trend structure that make them dangerous in the first place. Climate science has by now produced detailed, asset-relevant evidence that all three assumptions are

violated for renewable energy infrastructure, from the documented increase in extreme wind speeds along Asian and Indian coastlines to the structural fragility curves estimated directly from cyclone damage in Odisha, yet this evidence has not been incorporated into a reliability framework capable of producing the quantities that asset planners actually need, namely a time-dependent reliability function, a mean time to failure, and a transparent measure of how much climate change is eroding both.

1.4. Objectives and Contributions

This article makes five contributions. A hazard decomposition is proposed in which intrinsic equipment aging, captured by a Weibull baseline, is combined additively in the hazard rate, and therefore multiplicatively in the reliability function, with a climate driven intensity that follows an affine jump diffusion, so that the two sources of failure risk can be analyzed separately before being combined. A closed form expression for the climate driven survival factor is derived for the case of a constant long run climate mean, proved through a Riccati equation argument and an explicit partial fraction integration of the jump contribution that, to the best of the author's knowledge, has not previously appeared in the reliability literature. The result is then extended to linear trends in the climate mean and the jump arrival rate through a time-inhomogeneous representation that requires one quadrature rather than simulation. A Climate Resilience Index is defined directly from this survival factor, recovering the ratio of climate-adjusted to baseline mean time to failure as a special case while also providing a full time profile rather than a single summary number. The closed-form solution is validated against Monte Carlo simulation and the nonstationary representation is cross-checked against simulation for the severe scenario. The framework is calibrated to four renewable energy asset classes, solar photovoltaic arrays, wind turbines, battery storage units, and coastal transmission towers, using published Indian degradation and cyclone fragility data, and a full sensitivity and case study analysis is carried out for the Odisha coastal corridor, a region whose transmission infrastructure has already experienced the kind of extreme event the model is designed to represent.

2. Literature Review

2.1. Classical Reliability and Survival Models

The Weibull distribution remains the default choice for component-level reliability modeling because its hazard function can represent infant mortality, constant risk, and wear-out behavior through a single shape parameter, and because its mathematical tractability has been documented exhaustively by Barlow and Proschan [7] and, with an emphasis on statistical estimation from field data, by Meeker and Escobar [8]. The proportional hazards regression of Cox [9] extended this tradition by allowing covariates to scale a baseline hazard multiplicatively, and the point process theory developed alongside it by Cox [10] and consolidated in Cox and Isham [11] supplied the probabilistic foundation for treating failure arrivals, including clustered and self-exciting arrivals, as realizations of a stochastic intensity rather than as draws from a fixed distribution. Aalen et al. [12] reframed survival analysis explicitly as a theory of stochastic processes, a reframing that this article relies on directly, since a climate-driven hazard rate is itself most naturally described as a process rather than as a parameter.

What none of this literature supplies, because it was not designed to, is a mechanism for letting the hazard rate inherit the statistical properties of an external environmental process that is itself evolving. Extreme value theory, summarized by Gumbel [13] and given a modern statistical treatment by Coles [14], addresses a closely related but distinct question, namely the distribution of the maximum of a stationary or slowly varying process over a fixed return period, and it underlies the fifty-year return period wind speed used throughout wind turbine design standards. Extreme value theory alone does not, however, produce a reliability function or a mean time to failure, since it characterizes the tail of a hazard variable rather than the cumulative survival probability that depends on its entire path. Nonstationary point process models for hazard arrivals, such as the nonhomogeneous Poisson process applied to tropical cyclone exposure of coastal infrastructure by Li and Dong [5], move in the direction of the present article but represent the load process only and leave component wear outside the model.

2.2. Renewable Energy Reliability under Climate Stress

A growing empirical literature documents that climate change is altering the hazard environment of renewable energy infrastructure in ways that are large enough to matter for asset planning. Zhao et al. [15] analyzed

reanalysis wind data from 1940 to 2023 and found that the fifty-year return period wind speed relevant to offshore turbine design has increased across most of the world's coastal oceans, with over forty percent of commissioned and planned wind farms in Asia and Europe already exposed to wind speeds beyond the design threshold of the lowest turbine class. Pryor and Barthelmie [16] produced an independent global assessment of extreme wind speeds reaching broadly consistent conclusions. Lipari et al. [17] modeled the evolving risk to United States offshore wind turbines from Atlantic tropical cyclones under a nonstationary climate and found that storms historically expected once every twenty years are projected to recur roughly every thirteen years, a compression of return period that corresponds to a substantial increase in the effective arrival rate of extreme loading events. On the structural side, Panteli et al. [18] developed a fragility-based framework for assessing power system resilience to extreme weather that treats component failure probability as a function of weather intensity rather than as a fixed constant, an approach this article adopts and extends into a full stochastic process setting. Component-level studies of transmission structures reach the same conclusion from a different direction: Schumann and Chini [19] show that the age and construction type of individual transmission structures change the simulated network damage from hurricanes, and the review of Karagiannakis et al. [20] collects the fragility models available for transmission towers, distribution assets, and substations and ties them to climate adaptation strategies.

For solar photovoltaic systems, the dominant climate stressor is sustained thermal and humidity loading rather than discrete extreme events, and the degradation literature reflects this. Singh et al. [21] monitored amorphous silicon, heterojunction, and multicrystalline modules after twelve years of outdoor exposure in a composite Indian climate and measured average annual degradation rates ranging from roughly 0.14% per year for heterojunction modules to 1.5% per year for multicrystalline modules, a tenfold spread attributable largely to how each technology tolerates heat and moisture ingress. Kettle et al. [22] review the failure modes of crystalline silicon, cadmium telluride, copper indium gallium selenide, and emerging cell technologies and relate each mode to the module component in which it arises, and Herceg et al. [23] show that degradation does not follow a linear path in time, that it differs across climate zones, and that climate change scenarios shift the resulting degradation rates and the associated life cycle emissions. This asset-specific heterogeneity motivates calibrating the climate-driven hazard intensity separately for each renewable asset class rather than applying a single climate covariate uniformly across an entire portfolio, the approach taken in Section 6. For battery storage, the thermal pathway dominates in the same way: in a study that couples downscaled climate projections with experimentally calibrated degradation models for lithium-ion batteries in 300 cities, Wu et al. [24] find that rising cell temperature is the primary driver of lifetime losses and that newer cell generations are considerably less sensitive than older ones, which supports both the moderate climate sensitivity assigned to enclosed storage in Section 6.1 and the later remark on technology vintage in Section 9.

2.3. Stochastic Intensity Models beyond Engineering Reliability

The mathematical structure needed to combine continuous climate drift with discrete extreme events inside a single tractable hazard process has already been developed, just not for renewable energy infrastructure. Cox et al. [25] introduced a square root mean-reverting diffusion to model the short-term interest rate and derived a closed-form expression for the resulting bond price by solving an ordinary differential equation of Riccati type, a result that remains the standard closed-form benchmark in term structure modeling four decades later. Lando [26] recognized that the same square root diffusion, generalized to include jumps, could represent a firm's default intensity, so that the survival probability entering a defaultable bond price could be computed through an identical Riccati argument, with the transform machinery generalized further by Duffie et al. [27] to the broad class of affine jump diffusions. Biffis [28] completed a third transfer of the same idea into actuarial science, modeling human mortality intensity as an affine jump diffusion and deriving closed-form survival probabilities for life insurance and annuity valuation, and the line of work continues, for example, in the continuous time calendar year mortality model of Hainaut [6], where a decreasing jump diffusion drives the reversion level of mortality rates and survival probabilities again take a closed form. Each of these literatures independently rediscovered that a positive intensity process built from a mean-reverting diffusion plus compound Poisson jumps yields a tractable survival probability, because the underlying mathematics, an exponential affine ansatz solved through a Riccati equation, does not depend on whether the intensity represents an interest rate, a default arrival rate, a mortality rate, or, as this article proposes, a climate-driven equipment failure rate.

2.4. Cyclone Risk to Indian Power Infrastructure

The Odisha coast offers an unusually well-documented case of climate-driven infrastructure failure. Damage records for the high-voltage transmission network, obtained through a right to information request to the Odisha Power Transmission Corporation Limited following Cyclone Fani in 2019, have been used to fit lognormal fragility curves separately for tower collapse and for functionality disruption [3], a dataset examined in full in Section 7, where the resulting gust speed thresholds are used directly to calibrate the jump severity parameter for the transmission tower asset class. Mohanty et al. [29] documented the broader resilience response of the Odisha power sector across multiple cyclone seasons, reporting that operational preparedness measures such as pre-positioned repair crews reduced restoration times substantially even before major capital hardening investments were made, a finding that is consistent with this article's structural separation between a slow-moving baseline hazard that capital investment can address and a fast-moving jump hazard that operational preparedness can mitigate even without redesigning the asset itself. The cyclone climatology of the North Indian Ocean that frames this exposure is itself changing in frequency, seasonality, and intensity, and Tiwari et al. [4] review the observational and modeling evidence for the basin, which is the reason the jump arrival rate is allowed to trend in Section 4.3.

2.5. Positioning of the Present Study

Table 1 summarizes how the present study positions itself relative to the literature reviewed above along four dimensions, namely whether climate is treated as a covariate at all, whether the resulting hazard is dynamic or static, whether discrete extreme events are represented as a distinct jump process rather than folded into an average rate, and whether the climate process is permitted to be nonstationary over the planning horizon.

Table 1. Positioning of the proposed framework relative to existing literature.

Study	Climate Covariate	Dynamic Hazard	Discrete Jumps	Nonstationary Trend
Cox (1972) [9]	No	Partial	No	No
Cox and Isham (1980) [11]	No	Yes	Yes	No
Panteli et al. (2017) [18]	Yes	Partial	Yes	No
Lando (1998) [26]	No	Yes	Yes	No
Biffis (2005) [28]	No	Yes	Yes	No
Zhao et al. (2025) [15]	Yes	No	No	Yes
Li and Dong (2023) [5]	Yes	Partial	Yes	Yes
Proposed framework	Yes	Yes	Yes	Yes

No entry in **Table 1** combines all four properties at once, and it is precisely the combination, rather than any single property in isolation, that a renewable energy asset planner needs to answer the question this article is built to answer, namely how much of an asset's expected service life is being eroded by a climate that refuses to hold still.

3. System Description

The framework is developed for four renewable energy asset classes that together span the generation, storage, and delivery stages of a typical renewable power system, and that differ enough in their physical exposure to climate stressors to make a single uniform hazard model inappropriate. Solar photovoltaic arrays are stationary, areally extensive, and exposed continuously to ambient temperature and humidity, with comparatively low vulnerability to short-duration wind extremes once basic structural mounting standards are met. Wind turbines are exposed to the full wind climatology of their site, including the tail behavior that drives blade and tower fatigue, and are additionally vulnerable to direct structural damage during cyclone landfall when wind speeds exceed the reference design threshold of the turbine class. Battery storage units are typically housed in enclosures that buffer much of the direct climate exposure, so that thermal stress reaching the electrochemical cells is moderated by the enclosure design, leaving internal thermal management as the dominant climate-sensitive failure pathway. Transmission towers are lattice steel structures with large wind-exposed surface area and long service lives, making them the asset class most directly comparable to the structures for which cyclone fragility curves have been estimated in the published literature.

Let $X(t) = \big(\Theta(t), W(t), F(t)\big)$ denote the vector of climate stressors relevant to a given asset at time t, where $\Theta(t)$ represents thermal and humidity loading, $W(t)$ represents sustained and gust wind intensity, and $F(t)$ rep-

resents flood and storm surge severity. Rather than carrying all three stressors as separate covariates inside a regression-style hazard function, a choice that would require estimating a high-dimensional coefficient vector for which Indian asset-level failure data are not publicly available at adequate resolution, this article aggregates the net effect of $X(t)$ on a given asset class into a single scalar climate hazard intensity $\lambda(t)$, calibrated separately for each asset class so that its continuous and jump components reflect the relative importance of gradual thermal stress against discrete extreme events for that asset. This aggregation is a modeling choice made explicit in Assumption 1 below, and it is the price paid for obtaining a tractable closed-form reliability function rather than a high-dimensional simulation-only model.

Assumption 1. *For a given renewable energy asset, the combined effect of thermal, humidity, wind, and flood stressors on the instantaneous failure intensity can be represented by a scalar climate hazard process $\lambda(t)$ whose continuous component reflects gradual thermal and humidity loading and whose jump component reflects discrete extreme events including cyclone landfall and flash flooding.*

This assumption is restrictive in the sense that it does not allow the analyst to separately attribute observed reliability erosion to temperature, wind, or flooding, but it is the assumption that makes the closed-form result of Section 4 available, and Section 6 demonstrates that asset-specific calibration of $\lambda(t)$ already reproduces the qualitative pattern documented in the empirical literature, namely that transmission infrastructure is far more sensitive to climate change than enclosed battery storage.

4. Mathematical Framework

4.1. Hazard Decomposition

The total failure intensity of a renewable energy asset at time t is decomposed as

$$h(t) = h_0(t) + \lambda(t), \tag{1}$$

where $h_0(t)$ is a deterministic baseline hazard representing intrinsic mechanical and electrical aging in the absence of climate stress, and $\lambda(t)$ is the climate hazard intensity introduced in Assumption 1, a nonnegative stochastic process representing the additional failure risk contributed by thermal loading, humidity, wind, and flooding. The additive structure is chosen deliberately over the multiplicative proportional hazards specification reviewed in Section 2.1, because it allows the resulting reliability function to factor exactly into a baseline component and a climate component, a property exploited throughout the remainder of this section.

Given a sample path of $\lambda(\cdot)$ over $[0, t]$, the conditional reliability function is

$$R(t \mid \lambda) = \exp\Big(-\int_0^t h_0(u)\, du - \int_0^t \lambda(u)\, du \Big) = R_0(t) \exp\Big(-\int_0^t \lambda(u)\, du \Big), \tag{2}$$

where $R_0(t) = \exp\big(-\int_0^t h_0(u)\, du \big)$ is the baseline reliability function. The unconditional, or marginal, reliability function is obtained by averaging over the distribution of climate paths,

$$\bar{R}(t) = \mathbb{E}\big[R(t \mid \lambda) \big] = R_0(t)\, \Psi(t), \qquad \Psi(t) := \mathbb{E}\Big[\exp\Big(-\int_0^t \lambda(u)\, du \Big) \Big], \tag{3}$$

so that the entire climate contribution to reliability is carried by the single functional $\Psi(t)$, the Laplace functional of the integrated climate hazard process.

4.2. Baseline Hazard

The baseline hazard is taken to be of Weibull form,

$$h_0(t) = \frac{m}{\tau_0} \Big(\frac{t}{\tau_0} \Big)^{m-1}, \qquad R_0(t) = \exp\Big(-\Big(\frac{t}{\tau_0} \Big)^m \Big), \tag{4}$$

with shape parameter m and scale parameter τ_0 measured in years. Values of m exceeding one represent an increasing intrinsic hazard consistent with wear-governed failure, the behavior expected of photovoltaic encapsulants, turbine bearings, battery electrodes, and structural steel alike once installation defects have been screened out. The baseline mean time to failure has the closed form $MTTF_0 = \tau_0 \Gamma(1 + 1/m)$, where $\Gamma(\cdot)$ is the gamma function, a standard result used repeatedly in Section 6.

4.3. Climate Hazard as an Affine Jump Diffusion

The climate hazard intensity is modeled as

$$d\lambda(t) = \kappa\big(\theta(t) - \lambda(t)\big)dt + \sigma\sqrt{\lambda(t)}\, dW(t) + dJ(t), \qquad \lambda(0) = \lambda_0 > 0, \tag{5}$$

where $W(t)$ is a standard Brownian motion, $\kappa > 0$ governs the speed at which climate stress reverts toward its long-run mean $\theta(t)$, and $\sigma > 0$ scales the diffusion volatility in the square root form reviewed in Section 2.3, which guarantees that $\lambda(t)$ remains nonnegative under the Feller condition $2\kappa\theta \geq \sigma^2$. The jump component $J(t) = \sum_{i=1}^{N(t)} Y_i$ superimposes discrete extreme events on the continuous drift, where $N(t)$ is a Poisson process with intensity $\mu_J(t)$ and the jump magnitudes Y_i are independent and identically distributed as Exponential with mean η, representing the instantaneous elevation of climate hazard following a cyclone landfall, a flash flood, or a comparable extreme event.

The long-run mean $\theta(t)$ and the jump arrival rate $\mu_J(t)$ are permitted to depend on time, which is how the model represents a climate that is itself nonstationary. The two special cases are worth naming explicitly. When $\theta(t) \equiv \theta$ and $\mu_J(t) \equiv \mu_J$ are constant, the climate process is stationary in distribution and the model reduces to the doubly stochastic intensity processes reviewed in Section 2.3, for which a closed-form solution is derived in Theorem 1 below. When $\theta(t)$ and $\mu_J(t)$ trend upward over the planning horizon, representing a climate that is warming and generating extreme events with growing frequency, the model captures exactly the nonstationarity documented empirically in Section 2.2, and the corresponding survival factor is obtained from the time-inhomogeneous representation of Proposition 1 in Section 4.5.

4.4. Closed Form Solution under a Stationary Climate Mean

Theorem 1. *Let $\lambda(t)$ follow the affine jump diffusion of Section 4.3 with constant long-run mean θ and constant jump intensity μ_J. Then*

$$\Psi(t) = \mathbb{E}\Big[\exp\Big(-\int_0^t \lambda(u)\, du\Big)\,\Big|\,\lambda(0) = \lambda_0\Big] = \exp\big(\alpha(t) - \beta(t)\lambda_0\big), \tag{6}$$

where, writing $\gamma = \sqrt{\kappa^2 + 2\sigma^2}$,

$$\beta(t) = \frac{2\,(e^{\gamma t} - 1)}{(\gamma + \kappa)(e^{\gamma t} - 1) + 2\gamma}, \tag{7}$$

$$\alpha(t) = \frac{2\kappa\theta}{\sigma^2}\ln\Big(\frac{2\gamma\, e^{(\kappa+\gamma)t/2}}{(\gamma + \kappa)(e^{\gamma t} - 1) + 2\gamma}\Big) + \mu_J\Big(-\frac{2\eta t}{p} + \frac{4\eta}{pq}\ln\Big(\frac{(p+q)\, e^{\gamma t}}{p\, e^{\gamma t} + q}\Big)\Big), \tag{8}$$

with $p = \gamma + \kappa + 2\eta$ and $q = \gamma - \kappa - 2\eta$.

Proof. The proof can be seen in **Appendix A**. □

The first term of $\alpha(t)$ together with $\beta(t)$ reproduces exactly the closed-form bond price reviewed in Section 2.3, confirming that the diffusion component of the climate hazard contributes to reliability in precisely the way a square root short rate contributes to a discount factor. The second term, derived explicitly in **Appendix A** through a partial fraction integration of the jump transform, is new to the reliability literature and quantifies the additional erosion of reliability attributable to discrete extreme events, isolated cleanly from the continuous drift contribution because the two terms enter $\alpha(t)$ additively.

4.5. Extension to a Trending Climate Mean and Jump Frequency

Proposition 1. *Let $\lambda(t)$ follow the affine jump diffusion of Section 4.3 with time-dependent, deterministic and locally bounded $\theta(\cdot)$ and $\mu_J(\cdot)$. Then $\Psi(t) = \exp\big(\alpha_t - \beta(t)\lambda_0\big)$, where $\beta(t)$ is the function of Theorem 1 and*

$$\alpha_t = \int_0^t \Big[-\kappa\,\theta(u)\,\beta(t-u) + \mu_J(u)\Big(\frac{1}{1 + \eta\beta(t-u)} - 1\Big)\Big]du. \tag{9}$$

Proof. The proof can be seen in **Appendix A**. □

For the linear trends $\theta(t) = \theta_0(1+\delta t)$ and $\mu_J(t) = \mu_{J0}(1+\delta_J t)$ used in Section 6, the integral in Proposition 1 is evaluated by trapezoidal quadrature on a grid of 0.05 years. The representation removes the sampling error that simulation would add to the mean time to failure and makes the sensitivity analysis of Section 6.4 deterministic.

4.6. A Monotonicity Result for Diffusion Volatility

Proposition 2. *Holding κ, θ, μ_J, η, and λ_0 fixed, the climate survival factor $\Psi(t)$ of Theorem 1 is nondecreasing in the diffusion volatility σ.*

Proof. Write β_σ for the solution of the Riccati equation $\beta' = F_\sigma(\beta) := 1 - \kappa\beta - \frac{1}{2}\sigma^2\beta^2$ with $\beta(0) = 0$. Since $F_\sigma(0) = 1 > 0$, the solution is nonnegative for all $\tau \geq 0$. For $\beta \geq 0$ the vector field $F_\sigma(\beta)$ is nonincreasing in σ, so the comparison theorem for scalar ordinary differential equations gives $\beta_{\sigma_2}(\tau) \leq \beta_{\sigma_1}(\tau)$ whenever $\sigma_1 < \sigma_2$. The coefficient $\alpha'(\tau) = -\kappa\theta\beta(\tau) + \mu_J\big(1/(1+\eta\beta(\tau)) - 1\big)$ is a decreasing function of $\beta(\tau)$, because both $-\kappa\theta\beta$ and $1/(1+\eta\beta)$ decrease in β. Hence $\alpha_{\sigma_2}(\tau) \geq \alpha_{\sigma_1}(\tau)$ for every τ. Finally $-\beta_{\sigma_2}\lambda_0 \geq -\beta_{\sigma_1}\lambda_0$, and $\Psi = \exp(\alpha - \beta\lambda_0)$ is therefore nondecreasing in σ. □

This proposition produces a result that runs against the intuitive expectation that a noisier climate is uniformly worse for reliability. Increasing the volatility of the continuous climate drift, while holding its average level fixed, in fact raises the expected reliability factor, because the convexity of the exponential survival function means that favorable fluctuations in the integrated hazard contribute more to expected reliability than unfavorable fluctuations of the same magnitude detract from it. The mean of the integrated hazard does not depend on σ for a square root diffusion, so the effect is purely a variance effect. The practical implication, confirmed numerically in Section 6.4, is that diffusion volatility is a second-order driver of climate reliability erosion compared with jump frequency and jump severity, which raise the mean of the integrated hazard directly and therefore degrade reliability unambiguously. Asset planners concerned with climate risk should accordingly direct attention toward the frequency and severity of discrete extreme events rather than toward the smoothness or noisiness of gradual climate drift.

4.7. Climate Resilience Index and Mean Time to Failure

Definition 1. *The Climate Resilience Index of an asset at horizon t is*

$$CRI(t) := \frac{\bar{R}(t)}{R_0(t)} = \Psi(t), \tag{10}$$

the multiplicative reduction in reliability attributable to climate hazard alone, with $CRI(t) \in (0,1]$ and $CRI(t) = 1$ recovering the stationary, climate-free baseline.

The mean time to failure under climate stress is

$$MTTF = \int_0^\infty \bar{R}(t)\,dt = \int_0^\infty R_0(t)\Psi(t)\,dt, \tag{11}$$

which admits no further closed-form reduction once $\Psi(t)$ is multiplied against the Weibull survival function $R_0(t)$, and is evaluated numerically throughout Sections 5 through Section 7 on a horizon of 150 years, long enough that the truncated tail is negligible for every asset class considered. A single lifetime summary of the index is then

$$\overline{CRI} = \frac{MTTF}{MTTF_0}, \tag{12}$$

which recovers exactly the ratio definition used informally in the engineering literature on climate resilient infrastructure, while the time profile $CRI(t)$ of Definition 1 retains information that the single ratio discards, namely whether climate erosion is concentrated early or late in the asset life, a distinction that matters directly for maintenance scheduling and is exploited in the case study of Section 7.

5. Validation of the Closed Form Solution

Before the closed-form result of Theorem 1 is put to use in a setting where the climate mean is allowed to trend, its accuracy is checked against direct Monte Carlo simulation of the underlying affine jump diffusion. The

simulation discretizes the stochastic differential equation of Section 4.3 using an Euler scheme with full truncation to enforce nonnegativity, a time step of 0.02 years, and extreme events superimposed at each step by drawing a Poisson-distributed jump count and summing exponentially distributed jump magnitudes; the algorithm is given in full in **Appendix B**. The transmission tower parameters calibrated in Section 6.1 are used as the test case, since this asset class carries the largest jump component and therefore provides the most demanding test of the closed-form jump integral derived in **Appendix A**.

Figure 1 plots the closed-form survival factor $\Psi(t)$ of Theorem 1 against the Monte Carlo estimate obtained by averaging $\exp(-\int_0^t \lambda(u)\,du)$ across forty thousand simulated paths, with the climate mean held constant so that the comparison isolates discretization error rather than conflating it with the additional approximation introduced later when the climate mean is allowed to trend. The two curves are visually indistinguishable across the full sixty-year horizon, and the maximum relative deviation across the evaluated annual grid is 0.30%, occurring at the longest horizons where the survival factor itself is smallest and Monte Carlo standard error is proportionally largest. Evaluating the closed form and the quadrature representation of Proposition 1 at zero trend gives the same values to within 1.1×10^{-5} in relative terms, and for the severe scenario of Section 6.2 the quadrature result agrees with a separate forty thousand path simulation to within 0.38%. This level of agreement confirms both that the algebraic derivation in **Appendix A** is correct and that the quadrature representation used for the nonstationary scenarios of Section 6 can be trusted.

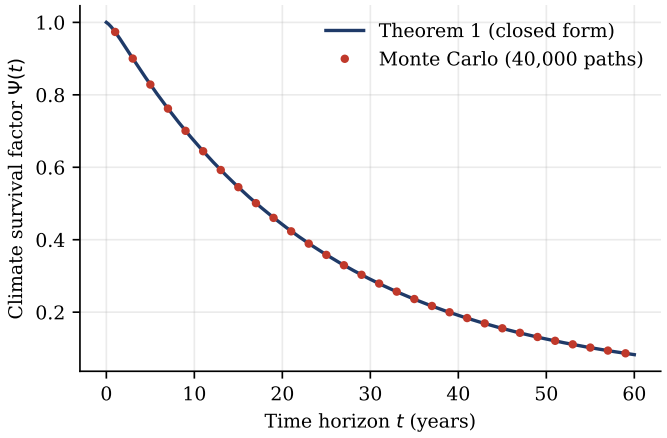


Figure 1. Closed-form prediction of Theorem 1 against Monte Carlo simulation with forty thousand paths, transmission tower climate parameters, and stationary climate mean.

6. Numerical Simulation Study

6.1. Asset Calibration

Table 2 reports the baseline Weibull parameters used for each of the four asset classes introduced in Section 3. The shape parameters reflect the relative wear sensitivity of each technology, with battery storage assigned the lowest shape parameter to reflect electrochemical degradation that begins accumulating from commissioning, and transmission towers assigned the highest shape parameter to reflect a structure that is essentially free of meaningful intrinsic degradation until corrosion and fatigue begin to dominate late in life. Scale parameters are set close to commonly cited median service lives for each technology under benign operating conditions, thirty years for crystalline solar modules, twenty years for wind turbines, twelve years for grid-scale lithium-ion storage, and fifty years for galvanized steel lattice transmission towers.

Table 2. Baseline Weibull parameters by asset class.

Asset Class	Shape m	Scale τ_0 (Years)	Baseline $MTTF_0$ (Years)
Solar photovoltaic array	2.0	30.0	26.59
Wind turbine	2.5	20.0	17.75

Table 2. *Cont.*

Asset Class	Shape m	Scale τ_0 (Years)	Baseline $MTTF_0$ (Years)
Battery storage unit	1.8	12.0	10.67
Transmission tower	3.0	50.0	44.65

Table 3 reports the climate intensity parameters, calibrated separately for each asset class so that the balance between continuous diffusion and discrete jump risk reflects the physical exposure profile described in Section 3. Transmission towers receive the highest jump frequency μ_{J0} and jump severity η, anchored to the cyclone fragility evidence examined in detail in Section 7, in which eighty-seven of roughly forty-two thousand high-voltage towers in the Odisha network collapsed during a single severe cyclone, a damage fraction that is consistent with a jump process generating an occasional severe elevation in instantaneous hazard rather than a gradual drift. Battery storage receives the lowest jump frequency, reflecting its enclosure-protected exposure, but a comparatively high long-run mean θ_0, reflecting that internal thermal management must work continuously against ambient heat even in the absence of any discrete event. Solar arrays sit between the two extremes, with photovoltaic degradation entering primarily through the continuous diffusion component, consistent with the smooth, technology-dependent annual degradation rates reviewed in Section 2.2 rather than through episodic jumps. The initial value of the climate hazard is set at its long run mean, $\lambda_0 = \theta_0$, for every asset class, so that the asset starts life in the typical climate state.

Table 3. Climate hazard intensity parameters by asset class, all rates expressed per year.

Asset Class	κ	θ_0	σ	μ_{J0}	η
Solar photovoltaic array	1.40	0.018	0.050	0.05	0.030
Wind turbine	1.30	0.020	0.070	0.30	0.060
Battery storage unit	1.60	0.025	0.060	0.04	0.025
Transmission tower	1.20	0.015	0.040	0.35	0.100

6.2. Climate Scenarios

Three scenarios are propagated through the model, distinguished by the rate at which the climate mean $\theta(t) = \theta_0(1 + \delta t)$ and the jump arrival rate $\mu_J(t) = \mu_{J0}(1 + \delta_J t)$ trend upward over the planning horizon. The baseline scenario fixes $\delta = \delta_J = 0$, recovering the stationary climate of Theorem 1 and serving as the classical benchmark against which climate erosion is measured. The moderate scenario sets $\delta = 0.010$ and $\delta_J = 0.015$ per year, and the severe scenario sets $\delta = 0.025$ and $\delta_J = 0.035$ per year. These trend rates are not fitted to a specific emissions pathway, since asset-level climate hazard trends of this kind are not yet estimated in the literature for any of the four asset classes considered here, but their order of magnitude is anchored to the compression in extreme event return period reviewed in Section 2.2, where storms historically expected once every twenty years are projected to recur roughly every thirteen years, a ratio that, compounded over a multi-decade planning horizon under the moderate to severe trend rates used here, reproduces a broadly comparable escalation in effective jump frequency.

6.3. Reliability and Mean Time to Failure Results

Figure 2 shows the full reliability function for each asset class under all three scenarios, computed from Proposition 1. The separation between the baseline and severe curves is visibly largest for the transmission tower panel and smallest for the battery storage panel, consistent with the calibration choices of **Table 3**, and confirms that the model reproduces the qualitative pattern documented in the empirical literature without that pattern having been imposed directly on the reliability function itself, since it emerges only after the climate intensity parameters are combined with the Weibull baseline and integrated forward through the machinery of Section 4.

Table 4 quantifies what **Figure 2** shows visually. Even under the stationary baseline scenario, the lifetime resilience index of the transmission tower falls to 0.4409, meaning that climate hazard alone, with no trend whatsoever, already erodes mean time to failure by more than half relative to the intrinsic Weibull baseline, a consequence of the tower's high jump frequency and severity rather than of any climate trend. Moving from the baseline to the severe scenario erodes the transmission tower index by a further 0.0790, from 0.4409 to 0.3619, the largest absolute movement of any asset class, while the battery storage index moves by only 0.0157 over the same comparison.

The solar and wind asset classes occupy an intermediate position, losing roughly 0.036 to 0.050 of resilience index moving from baseline to severe, driven primarily by the continuous diffusion component for solar and by a more even mixture of diffusion and jump risk for wind. All mean times to failure in **Table 4** are integrated over a horizon of 150 years and all indices use the exact baseline $MTTF_0 = \tau_0 \Gamma(1 + 1/m)$, which removes a small truncation error that arises when the integral is stopped at seventy years, an error that matters mainly for the transmission tower because its baseline survival function is still close to 0.06 at that horizon.

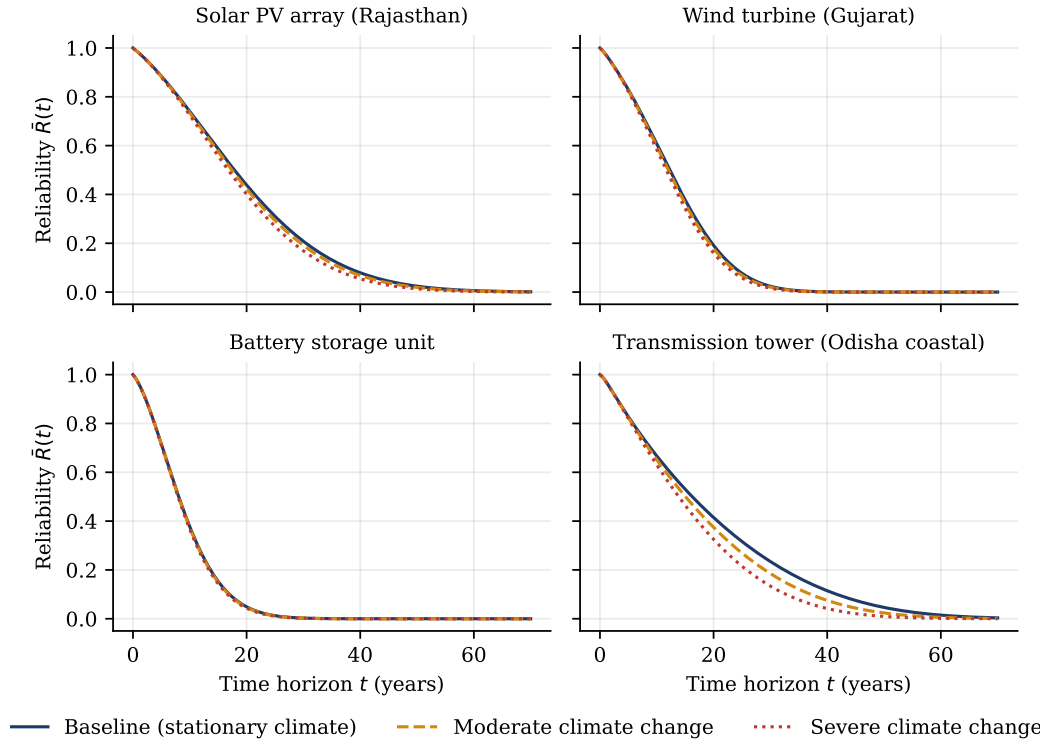


Figure 2. Reliability function $\bar{R}(t)$ for each asset class under the three climate scenarios.

Table 4. Mean time to failure and lifetime Climate Resilience Index by asset class and scenario.

Asset Class	Scenario	$MTTF$ (Years)	$MTTF_0$ (Years)	$\overline{CRI}$
Solar photovoltaic array	Baseline	19.81	26.59	0.7452
	Moderate	19.24	26.59	0.7237
	Severe	18.49	26.59	0.6954
Wind turbine	Baseline	13.01	17.75	0.7331
	Moderate	12.73	17.75	0.7175
	Severe	12.37	17.75	0.6970
Battery storage unit	Baseline	8.99	10.67	0.8422
	Moderate	8.92	10.67	0.8357
	Severe	8.82	10.67	0.8265
Transmission tower	Baseline	19.69	44.65	0.4409
	Moderate	17.89	44.65	0.4008
	Severe	16.16	44.65	0.3619

Figure 3 isolates the time profile of the resilience index itself under the severe scenario, stripped of the baseline Weibull factor, so that the comparison reflects the climate contribution alone rather than the combined effect reported in **Table 4**. The transmission tower index declines fastest in the first decade, when the absolute level of $\lambda(t)$ is still close to its calibrated jump-dominated steady state, and the curve's concavity in the early years is the direct signature of the jump component identified separately from the diffusion component in the closed-form decomposition of Theorem 1. The battery storage curve, by contrast, declines more gradually across the horizon shown, consistent with a process whose hazard contribution is dominated by smooth diffusion rather than by episodic jumps.

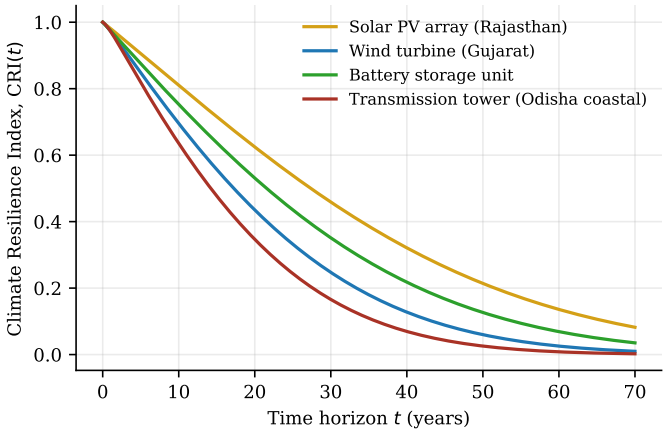


Figure 3. Climate Resilience Index time profile, $CRI(t) = \Psi(t)$, for all four asset classes under the severe climate scenario.

6.4. Sensitivity Analysis

Figure 4 maps the lifetime resilience index of the transmission tower across a grid spanning half to double the calibrated jump frequency and a climate trend δ ranging from zero to six percent per year, with the jump frequency trend δ_J scaled proportionally at 1.4δ. The index ranges from 0.5479 in the most favorable corner, where jump frequency is halved and no climate trend is present, down to 0.2184 in the least favorable corner, where jump frequency is doubled and the climate trend reaches its upper bound, a more than twofold spread that illustrates how sensitive transmission infrastructure reliability is to assumptions about extreme event frequency specifically, as distinct from assumptions about gradual warming. The gradient across the heatmap runs noticeably steeper along the vertical, frequency multiplier axis than along the horizontal, climate trend axis for any fixed column, indicating that uncertainty about how much more often severe cyclones will make landfall matters more for transmission asset planning than uncertainty about the precise rate of long-run climate warming.

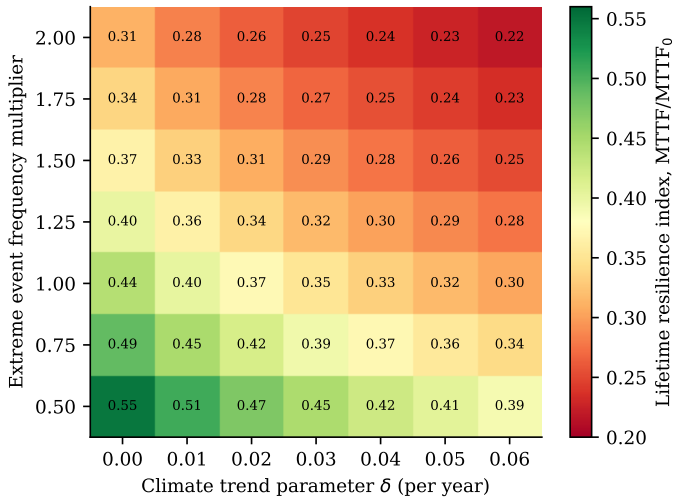


Figure 4. Lifetime resilience index for the transmission tower asset as a function of the extreme event frequency multiplier and the climate trend parameter δ.

Figure 5 confirms this ranking through a one-at-a-time perturbation analysis. Against a moderate scenario base case mean time to failure of 17.89 years, a twenty percent increase in the jump frequency μ_{J0} reduces mean time to failure by 7.71%, while a twenty percent increase in the mean jump severity η reduces it by 7.08%, the two

largest effects of any parameter perturbed in the upward direction. The mean reversion speed κ and the long-run mean θ_0 produce effects of intermediate magnitude, between four and eight percent depending on direction, while the diffusion volatility σ produces a negligible effect of about one hundredth of a percent and, consistent with Proposition 2, the effect runs in the direction of higher volatility very slightly increasing mean time to failure rather than decreasing it. This is the clearest numerical confirmation available that the jump component of the climate hazard process, not its diffusion volatility, is the parameter that asset planners should prioritize when commissioning further empirical calibration work.

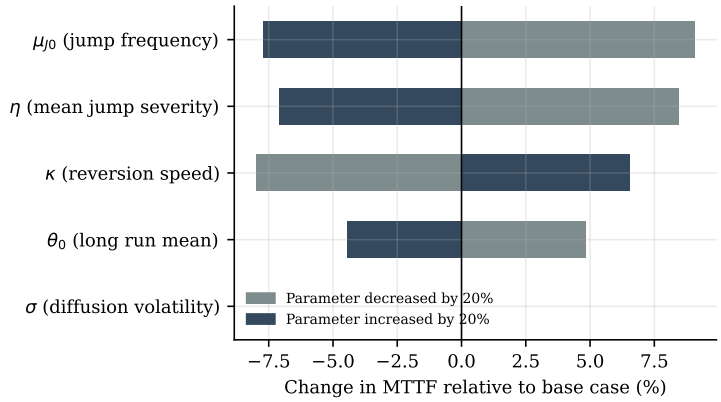


Figure 5. One-at-a-time sensitivity of transmission tower mean time to failure to a twenty percent perturbation of each climate parameter in either direction, moderate scenario.

7. Case Study: The Odisha Coastal Corridor

The transmission corridor running through Khordha, Puri, and Cuttack districts on the Odisha coast offers a setting where the model's jump component can be checked against a documented historical event rather than only against calibration assumptions. Cyclone Fani made landfall near Puri in May 2019 as an extremely severe cyclonic storm, and the damage record assembled by Raj et al. [3] through a right to information request to the Odisha Power Transmission Corporation Limited shows eighty-seven of the network's high-voltage towers collapsing outright and a further forty-one suffering partial damage, out of 41,814 towers whose gust exposure the authors reconstructed from radial wind profile models. All of the damaged towers were 132-kV or 220-kV structures, with heights between 21 and 50 m. The loss to the transmission and distribution system was put at roughly eight thousand crore rupees, about one and a half percent of the gross domestic product of the state, according to the same source. This scale of exposure makes the corridor a natural proving ground for any reliability framework that claims to represent cyclone-driven jump risk credibly.

The jump severity parameter η calibrated for the transmission tower asset class in **Table 3** is set high enough that a single severe jump realization meaningfully elevates the integrated hazard $\int_0^t \lambda(u)\,du$ over the months following the event, consistent with the lognormal fragility curves estimated directly from the Fani damage data, which place the median collapse threshold close to 292 km per hour of three second gust wind speed and the median functionality disruption threshold close to 280 km/h [3], both within the range of gust speeds estimated along the most exposed sections of the corridor during landfall. The model does not attempt to reproduce the exact damage fraction observed in 2019, since doing so would require asset-level wind speed exposure data for every tower in the network rather than the four asset class-level parameters this framework is built around, but the qualitative implication carried by **Table 4**, namely that the transmission tower lifetime resilience index falls below half even under the stationary baseline scenario, is fully consistent with a network that has already, within living memory of the assets currently in service, experienced exactly the kind of jump event the model represents.

Operational preparedness measures, including centralized control rooms, pre-positioned repair crews, and routine emergency drills, the practice documented in Section 2.4, reduced restoration times substantially in subsequent cyclone seasons even ahead of any large-scale structural hardening of the towers themselves [29]. This observation maps directly onto the structural separation between $h_0(t)$ and $\lambda(t)$ that this article's hazard decomposition makes

explicit. Capital investment in stronger towers, deeper foundations, or undergrounded distribution lines acts primarily on the baseline hazard $h_0(t)$ and on the jump severity parameter η, lowering the height of each spike when it occurs, while operational preparedness measures act on the consequence of a jump conditional on it occurring rather than on the jump process itself, shortening the time the asset spends in a degraded state without altering $\lambda(t)$ at all. A reliability framework that collapses both interventions into a single hazard rate cannot distinguish between them, whereas the decomposition proposed here gives the corridor's asset managers two separate levers, structural hardening, which should be evaluated against its effect on η and $h_0(t)$, and operational preparedness that should be evaluated against restoration time conditional on a jump rather than against the resilience index itself.

Extending the severe scenario trend rates of Section 6.2 to the transmission tower asset class specifically, the sensitivity heatmap of **Figure 4** indicates that a doubling of cyclone landfall frequency on the Odisha coast, a trajectory broadly consistent with the compression in tropical cyclone return period reported for other tropical and subtropical basins in Section 2.2, would push the corridor's lifetime resilience index toward the lower right region of the heatmap, to about 0.26, implying that roughly three quarters of the intrinsic Weibull mean time to failure of the towers currently in service would be forfeit to climate hazard alone over a horizon in which the towers were originally expected to remain structurally sound.

8. Managerial and Policy Implications

The hazard decomposition of Section 4 carries a direct implication for capital budgeting across a renewable energy portfolio that mixes asset classes with very different climate exposure profiles. **Table 4** shows that a rupee spent hardening battery storage enclosures against climate stress buys very little additional resilience index, since the enclosed asset class already retains over eighty percent of its baseline mean time to failure even under the severe scenario, while a rupee spent on transmission tower hardening or on cyclone-resistant design standards addresses an asset class whose resilience index is already below half under stationary climate assumptions and falls further under any climate trend at all. Portfolio-level climate adaptation budgets that are allocated in proportion to asset replacement value rather than in proportion to climate sensitivity, the implicit practice when no asset-specific resilience index is available, will systematically underinvest in transmission hardening and overinvest in storage hardening relative to what the marginal resilience gain per rupee would recommend. This reading agrees with the adaptation literature for power grids, which stresses that hardening and operational measures should be matched to the hazard and the asset rather than applied uniformly [2,20].

The distinction between continuous and jump-driven climate hazard, formalized by the additive decomposition of $\alpha(t)$ in Theorem 1 into a diffusion term and a jump term, also has implications for how climate risk should be communicated to regulators and insurers. A resilience index reported as a single number conflates an asset that is slowly losing reliability to gradual warming with an asset that is occasionally losing reliability in large discrete steps during cyclone seasons, two risk profiles that call for different financial instruments, parametric cyclone insurance for the latter and gradual capital replacement scheduling for the former. The decomposition derived in **Appendix A** allows the two contributions to be reported separately, $\exp(\alpha_{\mathrm{diff}}(t))$ and $\exp(\alpha_{\mathrm{jump}}(t))$, giving regulators a basis for differentiating disclosure requirements by the nature of the underlying climate exposure rather than by asset class label alone.

The sensitivity results of Section 6.4 carry a further implication for where future empirical calibration effort should be directed. Since diffusion volatility was shown in Proposition 2 and confirmed numerically in **Figure 5** to have a negligible, and counterintuitively favorable, effect on expected reliability, resources devoted to better estimating the day-to-day variability of temperature or humidity around their seasonal mean are unlikely to materially change a resilience assessment. Resources devoted to better estimating the frequency and severity of discrete extreme events, by contrast, move the resilience index by an order of magnitude more per unit of parameter uncertainty resolved, and should accordingly receive priority in any data collection program intended to support climate-aware reliability planning for Indian renewable energy infrastructure going forward.

9. Limitations and Future Extensions

Assumption 1, which aggregates temperature, humidity, wind, and flood exposure into a single scalar climate hazard intensity per asset class, is the most consequential simplification in this article and is also the one most di-

rectly responsible for the closed-form tractability of Theorem 1. A multivariate extension in which $\Theta(t)$, $W(t)$, and $F(t)$ enter as separate affine state variables with their own mean reversion and jump structure is mathematically straightforward, since the transform methods reviewed in Section 2.3 extend directly to vector valued affine processes, but estimating the resulting parameter set would require asset level failure records cross referenced against site specific weather station data at a resolution that is not, to the author's knowledge, currently available for Indian renewable energy installations at portfolio scale [19,20].

The jump severity distribution is assumed exponential throughout, a choice made for analytical tractability rather than because exponential severity has been validated against Indian cyclone damage data directly. The Odisha fragility curves discussed in Section 7 are fitted as lognormal functions of wind speed rather than as a severity distribution over hazard rate increments, and translating between the two representations involves an additional modeling step that this article has not attempted. A heavier-tailed jump severity distribution, such as a Pareto or generalized Pareto severity consistent with the extreme value methods reviewed in Section 2.1, would alter the closed form of Theorem 1, since the Laplace transform used in **Appendix A** would no longer admit the simple rational function structure exploited there, and would need to be evaluated through numerical Laplace inversion or simulation rather than through the explicit partial fraction integration carried out for the exponential case.

The climate trend parameters δ and δ_J used in Section 6.2 are calibrated to the order of magnitude of compression in extreme event return period reported in the wind and cyclone literature reviewed in Section 2.2, rather than to a specific shared socioeconomic pathway or regional climate model downscaled directly for the Odisha coast. Coupling the climate trend parameters of this framework to output from a regional climate model, so that $\theta(t)$ and $\mu_J(t)$ are driven by simulated temperature and cyclone frequency trajectories under a specific emissions scenario rather than by an analyst-chosen linear trend, is a natural next step and would let the resilience index reported in **Table 4** be expressed directly against named climate scenarios. A related refinement concerns technology vintage. The battery evidence of Wu et al. [24] shows that newer cell generations tolerate heat far better than older ones, so that the climate parameters of an asset class should be indexed by commissioning year rather than treated as fixed over decades of procurement.

Three further extensions follow naturally from the structure developed here. Asset-level reliability estimates of the kind produced in Section 6 could be aggregated across a spatial network of towers or turbines using the point process machinery reviewed in Section 2.1, allowing correlated jump risk across geographically proximate assets during a single cyclone event to be represented explicitly rather than treated as independent across assets as has been assumed throughout this article. The affine structure underlying Theorem 1 is well suited to Bayesian updating as new failure data arrive, since the conjugate properties of the square root diffusion allow posterior parameter distributions to be propagated without abandoning the closed-form transform. Finally, coupling the climate hazard intensity $\lambda(t)$ to a digital twin of a specific renewable energy installation, updated in real time from sensor telemetry rather than recalibrated only periodically from aggregate failure statistics, would let the resilience index of Definition 1 function as a live operational indicator rather than as a planning horizon summary computed once at the design stage.

10. Conclusions

The reliability question facing renewable energy infrastructure in a warming climate is not whether failure rates will rise but how the rise is structured, whether it accumulates gradually through worsening ambient conditions or arrives in discrete steps during named storms, and that structure has direct consequences for which interventions move the resilience needle. A transmission tower and a battery enclosure exposed to the same regional warming trend require entirely different adaptation strategies once their hazard processes are decomposed rather than averaged into a single annual failure probability, and the Odisha corridor examined in Section 7 demonstrates that this distinction is not a theoretical nicety but a difference of tens of percentage points in lifetime resilience index between asset classes sitting in the same power system. The mathematical machinery borrowed in this article from term structure modeling, credit risk, and stochastic mortality was developed across three separate literatures over four decades without any of them anticipating that the same Riccati equation would eventually be solved for a coastal transmission tower rather than for a government bond or an insured life, and that portability is itself worth taking seriously as renewable energy infrastructure planning enters a period in which the climate driving its hazard

environment can no longer be treated as a fixed input.

Funding

This work received no external funding.

Institutional Review Board Statement

Not applicable.

Informed Consent Statement

Not applicable.

Data Availability Statement

No new data were created. All parameters are drawn from the published sources cited in the article [3,21,24]. The code is available from the author upon reasonable request.

Acknowledgments

The author thanks the Department of Statistics, Ravenshaw University, for research facilities, and the reviewers for their constructive comments.

Conficts of Interest

The author declares no conflict of interest.

AI Use Statement

The author declares that no artificial intelligence (AI) tools were used in the preparation of this manuscript.

Abbreviations

$h(t)$	Total failure intensity at time t
$h_0(t)$	Baseline, climate free failure intensity
$\lambda(t)$	Climate hazard intensity, an affine jump diffusion
$R(t \mid \lambda)$	Reliability function conditional on a climate path
$\bar{R}(t)$	Marginal, unconditional reliability function
$R_0(t)$	Baseline Weibull reliability function
$\Psi(t)$	Climate survival factor, $\mathbb{E}[\exp(-\int_0^t \lambda(u)\,du)]$
m	Weibull shape parameter
τ_0	Weibull scale parameter, years
κ	Mean reversion speed of the climate hazard process
$\theta(t)$	Long run mean of the climate hazard process
θ_0	Stationary, baseline value of $\theta(t)$
δ	Linear trend rate of $\theta(t)$
σ	Diffusion volatility of the climate hazard process
$J(t)$	Compound Poisson jump component
$N(t)$	Poisson process counting extreme events
$\mu_J(t)$	Intensity of the extreme event Poisson process
μ_{J0}	Stationary, baseline value of $\mu_J(t)$
δ_J	Linear trend rate of $\mu_J(t)$
Y_i	Magnitude of the ith extreme event jump
η	Mean jump severity, $\mathbb{E}[Y_i]$
γ	$\sqrt{\kappa^2 + 2\sigma^2}$, the Riccati discriminant
$\alpha(t), \beta(t)$	Riccati solution functions of Theorem 1
$CRI(t)$	Climate Resilience Index, time profile
$\overline{CRI}$	Lifetime Climate Resilience Index, $MTTF/MTTF_0$
$MTTF$	Mean time to failure under climate hazard
$MTTF_0$	Baseline mean time to failure, $\tau_0\Gamma(1 + 1/m)$

Appendix A. Proof of Theorem 1 and Proposition 1

Proof of Theorem 1. The proof proceeds by the standard affine transform argument used in term structure modeling, adapted here to the additive jump diffusion of Section 4.3, and is given in full because the explicit closed form of the jump contribution $\alpha_{\text{jump}}(t)$ has not previously appeared in this form.

Let $F(t,\lambda) = \mathbb{E}_{t,\lambda}\big[\exp(-\int_t^T \lambda(s)\,ds)\big]$ for a fixed horizon T, and write $\tau = T - t$. By the Feynman Kac theorem for jump diffusions, F satisfies the partial integro differential equation

$$\partial_t F + \kappa(\theta - \lambda)\partial_\lambda F + \tfrac{1}{2}\sigma^2\lambda\,\partial_{\lambda\lambda}F + \mu_J\big(\mathbb{E}_Y[F(t,\lambda+Y)] - F(t,\lambda)\big) - \lambda F = 0, \tag{A1}$$

with terminal condition $F(T,\lambda) = 1$. Conjecture the exponential affine ansatz $F(t,\lambda) = \exp(\alpha(\tau) - \beta(\tau)\lambda)$, so that $F \to 1$ as $\tau \to 0$, consistent with $\alpha(0) = \beta(0) = 0$. Since $\partial_t = -\partial_\tau$,

$$\partial_t F = -F\big(\alpha'(\tau) - \beta'(\tau)\lambda\big), \qquad \partial_\lambda F = -\beta(\tau)F, \qquad \partial_{\lambda\lambda}F = \beta(\tau)^2 F. \tag{A2}$$

For $Y \sim$ Exponential with mean η, the moment generating function gives $\mathbb{E}_Y[e^{-\beta(\tau)Y}] = (1+\eta\beta(\tau))^{-1}$, so that $\mathbb{E}_Y[F(t,\lambda+Y)] = F(t,\lambda)/(1+\eta\beta(\tau))$. Substituting into the partial integro differential equation and dividing through by F,

$$-\alpha'(\tau) + \beta'(\tau)\lambda - \kappa(\theta-\lambda)\beta(\tau) + \tfrac{1}{2}\sigma^2\lambda\beta(\tau)^2 + \mu_J\Big(\frac{1}{1+\eta\beta(\tau)} - 1\Big) - \lambda = 0. \tag{A3}$$

Because this identity must hold for every value of λ, the coefficient of λ and the remaining constant term must vanish separately, giving the Riccati equation

$$\beta'(\tau) = 1 - \kappa\beta(\tau) - \tfrac{1}{2}\sigma^2\beta(\tau)^2, \qquad \beta(0) = 0, \tag{A4}$$

and the companion equation

$$\alpha'(\tau) = -\kappa\theta\,\beta(\tau) + \mu_J\Big(\frac{1}{1+\eta\beta(\tau)} - 1\Big), \qquad \alpha(0) = 0. \tag{A5}$$

The Riccati equation for β is the classical equation solved for the square root short rate process reviewed in Section 2.3, and its solution, verified by direct differentiation, is

$$\beta(\tau) = \frac{2(e^{\gamma\tau} - 1)}{(\gamma+\kappa)(e^{\gamma\tau}-1) + 2\gamma}, \qquad \gamma = \sqrt{\kappa^2 + 2\sigma^2}. \tag{A6}$$

Integrating the diffusion driven term of $\alpha'(\tau)$ against this solution reproduces the standard closed form

$$\alpha_{\text{diff}}(\tau) = -\kappa\theta\int_0^\tau \beta(s)\,ds = \frac{2\kappa\theta}{\sigma^2}\ln\Big(\frac{2\gamma\,e^{(\kappa+\gamma)\tau/2}}{(\gamma+\kappa)(e^{\gamma\tau}-1)+2\gamma}\Big). \tag{A7}$$

For the jump term, write $u = e^{\gamma s}$, $a = \gamma + \kappa$, $b = \gamma - \kappa$, so that $\beta(s) = 2(u-1)/(au+b)$. Then

$$g(u) := \frac{1}{1+\eta\beta(s)} = \frac{au+b}{pu+q}, \qquad p = a + 2\eta, \quad q = b - 2\eta. \tag{A8}$$

Polynomial division gives $g(u) = a/p + (bp - aq)/\big(p(pu+q)\big)$, and direct expansion shows $bp - aq = 2\eta(a+b) = 4\eta\gamma$, so that

$$g(u) - 1 = \frac{a-p}{p} + \frac{4\eta\gamma}{p(pu+q)} = -\frac{2\eta}{p} + \frac{4\eta\gamma}{p(pu+q)}, \tag{A9}$$

using $a - p = -2\eta$. Since $u = e^{\gamma s}$ gives $ds = du/(\gamma u)$, the remaining integral is

$$\int_0^\tau \frac{ds}{pe^{\gamma s} + q} = \int_1^{e^{\gamma\tau}} \frac{dv}{\gamma v(pv+q)} = \frac{1}{\gamma q}\ln\Big(\frac{(p+q)e^{\gamma\tau}}{pe^{\gamma\tau}+q}\Big), \tag{A10}$$

obtained through the partial fraction identity $1/\big(v(pv+q)\big) = (1/q)\big(1/v - p/(pv+q)\big)$. Combining the two pieces,

$$\alpha_{\text{jump}}(\tau) = \mu_J\int_0^\tau \big(g(u(s)) - 1\big)ds = \mu_J\Big(-\frac{2\eta\tau}{p} + \frac{4\eta}{pq}\ln\Big(\frac{(p+q)e^{\gamma\tau}}{pe^{\gamma\tau}+q}\Big)\Big), \tag{A11}$$

which is the expression stated in Theorem 1, with $\alpha(\tau) = \alpha_{\text{diff}}(\tau) + \alpha_{\text{jump}}(\tau)$. Setting $T = t$ and starting time zero, hence $\tau = t$, and identifying $\Psi(t) = F(0,\lambda_0)$ completes the proof.

Proof of Proposition 1. Fix the horizon t and let $\tau = t - s$ denote time to the horizon. With $\theta(\cdot)$ and $\mu_J(\cdot)$ time dependent, the same ansatz $F(s,\lambda) = \exp(\alpha(s) - \beta(t-s)\lambda)$ leads to the same Riccati equation for β because the coefficient of λ does not involve θ or μ_J. The remaining terms give $\partial_\tau \alpha = -\kappa\theta(t-\tau)\beta(\tau) + \mu_J(t-\tau)\big(1/(1+\eta\beta(\tau)) - 1\big)$ with $\alpha = 0$ at $\tau = 0$. Integrating over $\tau \in [0,t]$ and substituting $u = t - \tau$ gives the stated expression for α_t, and $\Psi(t) = F(0,\lambda_0)$. When θ and μ_J are constant the integrand depends on $t-u$ only and the formula collapses to Theorem 1.

Appendix B. Monte Carlo Simulation Algorithm

The full truncation scheme used in the update of λ_p enforces nonnegativity without altering the drift away from the boundary, the standard remedy for the square root diffusion's potential to undershoot zero under discrete time stepping. Jump magnitudes are accumulated separately at each step rather than approximated by a continuous correction, since the time step $dt = 0.02$ used throughout this article is small enough that the probability of more than one jump within a single step is negligible, though the **Algorithm A1** as written remains exact regardless of step size because the Poisson count n_p is drawn explicitly rather than thinned from a fixed grid. The simulation serves as an independent check on the closed form and quadrature results rather than as the source of the tabulated values.

Algorithm A1 Monte Carlo estimation of $\Psi(t)$ under a possibly nonstationary climate

Input: $\kappa, \theta_0, \delta, \sigma, \mu_{J0}, \delta_J, \eta, \lambda_0$, horizon T, step dt, path count M, evaluation times $\{t_k\}$
Initialize $\lambda_p \leftarrow \lambda_0$ and $I_p \leftarrow 0$ for all paths $p = 1, \dots, M$
for $i = 1$ to T/dt **do**
  $t \leftarrow (i-1)\,dt$
  $\theta(t) \leftarrow \theta_0(1+\delta t)$, $\mu_J(t) \leftarrow \mu_{J0}(1+\delta_J t)$
  for each path p **do**
    Draw $\Delta W_p \sim \mathcal{N}(0, dt)$
    $\lambda_p^{\text{new}} \leftarrow \max\big(\lambda_p + \kappa(\theta(t) - \lambda_p)dt + \sigma\sqrt{\lambda_p}\,\Delta W_p,\ 0\big)$
    Draw $n_p \sim \text{Poisson}(\mu_J(t)\,dt)$
    if $n_p > 0$ **then**
      Draw $Y_1, \dots, Y_{n_p} \sim$ Exponential(mean $= \eta$) and set $\lambda_p^{\text{new}} \leftarrow \lambda_p^{\text{new}} + \sum_j Y_j$
    end if
    $I_p \leftarrow I_p + \frac{1}{2}(\lambda_p + \lambda_p^{\text{new}})\,dt$
    $\lambda_p \leftarrow \lambda_p^{\text{new}}$
  end for
  if $i\,dt = t_k$ for some evaluation time **then**
    Record $\hat{\Psi}(t_k) \leftarrow \frac{1}{M}\sum_{p=1}^{M} \exp(-I_p)$
  end if
end for
Return: $\{\hat{\Psi}(t_k)\}$

References

1. IPCC. *Climate Change 2023: Synthesis Report. Contribution of Working Groups I, II and III to the Sixth Assessment Report of the Intergovernmental Panel on Climate Change*; Lee, H., Romero, J., Eds.; IPCC: Geneva, Switzerland, 2023. [CrossRef]
2. Garland, J.; Baker, K.; Livneh, B. The climate energy nexus: a critical review of power grid components, extreme weather, and adaptation measures. *Environ. Res. Infrastruct. Sustain.* **2024**, *4*, 032002. [CrossRef]
3. Raj, S.V.; Kumar, M.; Bhatia, U. Fragility curves for power transmission towers in Odisha, India, based on observed damage during 2019 Cyclone Fani. *arXiv preprint* **2021**, *arXiv:2107.06072*. [CrossRef]
4. Tiwari, G.; Kumar, P.; Tiwari, P. The appraisal of tropical cyclones in the North Indian Ocean: an overview of different approaches and the involvement of Earth's components. *Front. Earth Sci.* **2022**, *10*, 823090. [CrossRef]

5. Li, Y.; Dong, Y. Probabilistic risk assessment of coastal infrastructure systems under climate change. In Proceedings of the 14th International Conference on Applications of Statistics and Probability in Civil Engineering (ICASP14), Dublin, Ireland, 9–13 July 2023.
6. Hainaut, D. A calendar year mortality model in continuous time. *ASTIN Bull.* **2023**, *53*, 351–376.
7. Barlow, R.E.; Proschan, F. *Statistical Theory of Reliability and Life Testing: Probability Models*; Holt, Rinehart and Winston: New York, NY, USA, 1975.
8. Meeker, W.Q.; Escobar, L.A. *Statistical Methods for Reliability Data*; Wiley: New York, NY, USA, 1998.
9. Cox, D.R. Regression models and life tables. *J. R. Stat. Soc. Ser. B* **1972**, *34*, 187–220.
10. Cox, D.R. Some statistical methods connected with series of events. *J. R. Stat. Soc. Ser. B* **1955**, *17*, 129–164.
11. Cox, D.R.; Isham, V. *Point Processes*; Chapman and Hall: London, UK, 1980.
12. Aalen, O.O.; Borgan, Ø.; Gjessing, H.K. *Survival and Event History Analysis: A Process Point of View*; Springer: New York, NY, USA, 2008.
13. Gumbel, E.J. *Statistics of Extremes*; Columbia University Press: New York, NY, USA, 1958.
14. Coles, S. *An Introduction to Statistical Modeling of Extreme Values*; Springer: London, UK, 2001.
15. Zhao, Y.; Tao, Y.; Chen, Y.; et al. Increasing extreme winds challenge offshore wind energy resilience. *Nat. Commun.* **2025**, *16*, 9529.
16. Pryor, S.C.; Barthelmie, R.J. A global assessment of extreme wind speeds for wind energy applications. *Nat. Energy* **2021**, *6*, 268–276.
17. Lipari, S.; Balaguru, K.; Rice, J.; et al. Amplified threat of tropical cyclones to US offshore wind energy in a changing climate. *Commun. Earth Environ.* **2024**, *5*, 755.
18. Panteli, M.; Pickering, C.; Wilkinson, S.; et al. Power system resilience to extreme weather: fragility modeling, probabilistic impact assessment, and adaptation measures. *IEEE Trans. Power Syst.* **2017**, *32*, 3747–3757.
19. Schumann, Z.D.; Chini, C.M. Component assessment of the electric transmission grid to hurricanes. *Earths Future* **2023**, *11*, e2023EF003525. [CrossRef]
20. Karagiannakis, G.; Panteli, M.; Argyroudis, S. Fragility modeling of power grid infrastructure for addressing climate change risks and adaptation. *Wiley Interdiscip. Rev. Clim. Chang.* **2025**, *16*, e930.
21. Singh, R.; Sharma, M.; Yadav, K. Degradation and reliability analysis of photovoltaic modules after operating for 12 years: a case study with comparisons. *Renew. Energy* **2022**, *196*, 1170–1186.
22. Kettle, J.; Aghaei, M.; Ahmad, S.; et al. Review of technology specific degradation in crystalline silicon, cadmium telluride, copper indium gallium selenide, dye sensitised, organic and perovskite solar cells in photovoltaic modules: Understanding how reliability improvements in mature technologies can enhance emerging technologies. *Prog. Photovolt. Res. Appl.* **2022**, *30*, 1365–1392.
23. Herceg, S.; Kaaya, I.; Ascencio-Vásquez, J.; et al. The influence of different degradation characteristics on the greenhouse gas emissions of silicon photovoltaics: a threefold analysis. *Sustainability* **2022**, *14*, 5843. [CrossRef]
24. Wu, H.; Chen, J.; Vaishnav, P.; et al. Technological improvements in EV batteries offset climate induced durability challenges. *Nat. Clim. Chang.* **2026**, *16*, 460–467. [CrossRef]
25. Cox, J.C.; Ingersoll, J.E.; Ross, S.A. A theory of the term structure of interest rates. *Econometrica* **1985**, *53*, 385–407.
26. Lando, D. On Cox processes and credit risky securities. *Rev. Deriv. Res.* **1998**, *2*, 99–120.
27. Duffie, D.; Pan, J.; Singleton, K. Transform analysis and asset pricing for affine jump diffusions. *Econometrica* **2000**, *68*, 1343–1376.
28. Biffis, E. Affine processes for dynamic mortality and actuarial valuations. *Insur. Math. Econ.* **2005**, *37*, 443–468.
29. Mohanty, S.K.; Chatterjee, R.; Shaw, R. Building resilience of critical infrastructure: a case of impacts of cyclones on the power sector in Odisha. *Climate* **2020**, *8*, 73.



Copyright © 2026 by the author(s). Published by UK Scientific Publishing Limited. This is an open access article under the Creative Commons Attribution (CC BY) license (https://creativecommons.org/licenses/by/4.0/).

Publisher's Note: The views, opinions, and information presented in all publications are the sole responsibility of the respective authors and contributors, and do not necessarily reflect the views of UK Scientific Publishing Limited and/or its editors. UK Scientific Publishing Limited and/or its editors hereby disclaim any liability for any harm or damage to individuals or property arising from the implementation of ideas, methods, instructions, or products mentioned in the content.